Nonlinear Biconstituent Diffusion: A Possible Trigger of Convection

JOSEPH T. SCHAEFER

National Severe Storms Laboratory, NOAA, Norman, Okla. 73069

(Manuscript received 16 January 1975, in revised form 18 July 1975)

ABSTRACT

Nonlinear biconstituent diffusion is proposed as a possible trigger for cumulus development. Properties of this second-order effect are examined. It is shown that this process can exist in the atmosphere and that it can produce sustained convective cells of appreciable magnitude. One possible atmospheric example is illustrated.

1. Introduction

Numerically modeled convective clouds are normally generated by introducing an initial perturbation into the hydro-thermodynamic fields describing a conditionally unstable atmosphere. These perturbations generally consist of the arbitrary specification of a temperature, water vapor or vertical velocity excess over a limited region within the simulated environment. This technique allows the study of growth and dissipation of subsequent convection, but its very nature excludes examination of the physics of cloud initiation.

While there are unquestionably myriad causes of cloud development, few have been numerically simulated. The South Dakota School of Mines Group (e.g., Orville and Sloan, 1970) has extensively studied the effect of orography on cloud initiation. Hill (1974) modeled cloud development caused by random fluctuations in a parameterized surface heating to determine the size and spacing of developing convective elements.

In this paper, a mechanism (which evolves from the independent diffusion of moisture and heat) by which convective currents can be initiated in an unperturbed, gravitationally stable environment is studied. Such conditions exist across a dryline (Schaefer, 1973). Observations via satellite imagery (Purdom, 1971) and aircraft (Fig. 1) reveal that this synoptic feature is often collocated with a band of cumulus clouds. These clouds are one possible atmospheric example of biconstituent convection.

2. The physical mechanism

While diffusion is generally a dissipative effect, in biconstituent fluids it can actually cause perturbations. One example of instability generated by diffusion is thermohaline convection (Baines and Gill, 1969). This process is generated by the double-diffusive effect arising from a viscously driven interaction between the fluid constituents of sea water (salt and heat). A density decrease with height in a multi-propertied fluid does not guarantee stability because diffusion can reorder the constituents so as to release the potential energy stored in the individual components. If the two properties have different diffusivities, linear theory can be used to show the development of organized currents (Turner, 1973).

However, even if the diffusivities (or eddy diffusivities) are identical, instabilities can occur when the constituent relationship for density is nonlinear. Such is the case in the atmosphere. Air density is directly related to the virtual potential temperature (T^*) which is a nonlinear combination of heat and moisture content. The defining equation is

$$T^*=\theta\left(\frac{1+q/0.622}{1+q}\right)\approx\theta(1+0.608q), \tag{1}$$

where θ is the potential temperature and q the mixing ratio. If diffusion is the only physical process considered and eddy-coefficient theory is assumed, the first law of thermodynamics and conservation of moisture are simply

$$\frac{\partial\theta}{\partial t}+\mathbf{v}\cdot\nabla\theta=K\nabla^2\theta, \tag{2}$$

$$\frac{\partial q}{\partial t}+\mathbf{v}\cdot\nabla q=K\nabla^2 q, \tag{3}$$

where t is time, $\mathbf{v}$ the vector velocity, and K the eddy diffusivity (assumed constant for simplicity). The Lewis number (ratio of eddy diffusivity to eddy conductivity) is assumed to be unity to exclude linear double-diffusive effects. Combining (2) and (3) through (1) gives the time rate of change of the virtual potential temperature:

$$\frac{\partial T^*}{\partial t}+\mathbf{v}\cdot\nabla T^*=K\nabla^2T^*-1.216K\nabla\theta\cdot\nabla q. \tag{4}$$

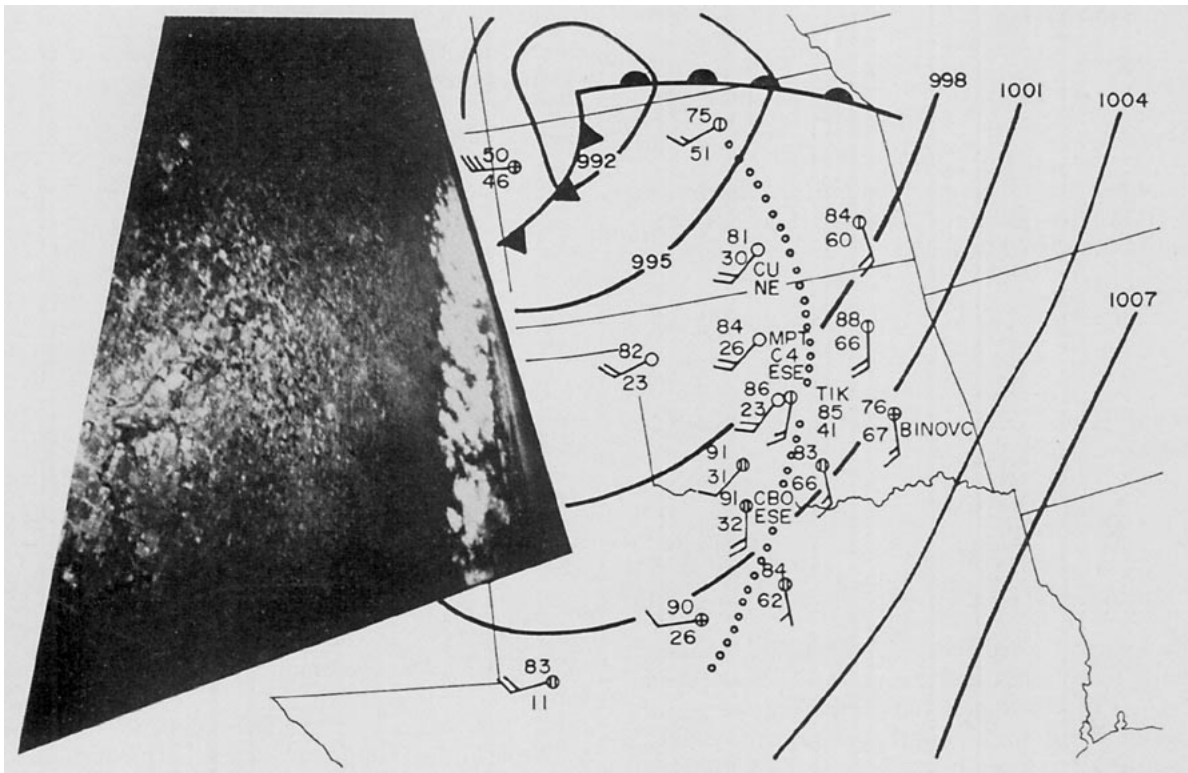

FIG. 1. A dryline as seen from an aircraft.

In the absence of motion, Eqs. (2) and (3) are simply diffusion equations and yield an exponential decay of any nonlinearities in the initial field. However the virtual potential temperature equation (4) contains an additional contribution which is a direct result of the nonlinear density relation. The right-hand sides of both constituent equations [(2) and (3)] are Fickian diffusion terms. With time each component configuration changes at a rate determined by its own distribution and is independent of that of the other component. Virtual potential temperature (density) changes at a rate proportional to the product of the constituent gradients. Thus, even if the virtual potential temperature field is initially uniform, it cannot maintain its spatial uniformity except for the trivial case when both constituents are independent of position. Thus in a nonlinear biconstituent system, diffusion acts to *create* density irregularities.

3. The nonlinear biconstituent diffusive effect

The potential effect of growth by diffusion in a nonlinear biconstituent medium can be seen by considering a hypothetical case of "creeping motion" (Reynolds number $\ll 1$). For such flows, inertia terms are negligible in comparison to viscous terms, and the velocity (v) can be omitted from the analysis (Schlichting, 1955). Further restricting the problem to two spatial dimensions yields diffusion equations of

$$\frac{\partial\theta}{\partial t}=K\left(\frac{\partial^2\theta}{\partial x^2}+\frac{\partial^2\theta}{\partial y^2}\right)=K\nabla_2{}^2\theta, \tag{2a}$$

$$\frac{\partial q}{\partial t}=K\nabla_2{}^2 q, \tag{3a}$$

$$\frac{\partial T^*}{\partial t}=K\nabla_2{}^2T^*-1.216K\boldsymbol{\nabla}_2\theta\cdot\boldsymbol{\nabla}_2 q. \tag{4a}$$

When these equations are combined with the definition of T^* [Eq. (1)] and proper initial and boundary conditions, a tractable system is obtained.

If the initial potential temperature distribution is simply a sinusoidal perturbation superimposed on a uniform field over an infinite domain, the general form of the solution of (2a) is

$$\theta=A+\theta_0 e^{-t/\tau}e^{i(kx+mz)}, \tag{5}$$

where

$$\tau=[K(k^2+m^2)]^{-1},$$

A and θ_0 are constants of integration, and k and m are the initial horizontal and vertical wavenumbers.

In the extreme case of an initially constant virtual potential temperature

$$T^*|_{t=0}=B=\text{constant}, \tag{6}$$

the initial mixing ratio field

$$q|_{t=0}=\left[\frac{B}{A}-1+\sum_{n=1}^{\infty}(-1)^n\left(\frac{B\theta_0{}^n}{A^{n+1}}\right)e^{in(kx+mz)}\right]0.608^{-1} \tag{6a}$$

can be obtained by dividing (5) into (6) and substituting from (1). Under this initial condition, (3a) can be immediately integrated to yield

$$q=\left[\frac{B}{A}-1+\sum_{n=1}^{\infty}(-1)^n\left(\frac{B\theta_0{}^n}{A^{n+1}}\right)e^{in(kx+mz)}e^{-n^2(t/\tau)}\right]0.608^{-1} \tag{7}$$

Thus the virtual potential temperature develops according to

$$T^*=B+\sum_{n=1}^{\infty}(-1)^nB\left(\frac{\theta_0}{A}\right)^{n+1}e^{i(n+1)(kx+mz)}$$
$$\times\{\exp[-(n^2+1)t/\tau]-\exp[-(n+1)^2t/\tau]\}. \tag{8}$$

Eqs. (5) and (7) depict exponential decays to uniform potential temperature and mixing ratio fields of A and $[(B/A)-1]/0.608$ respectively. However, owing to the diffusive mechanism, a perturbation actually develops in the virtual potential temperature field. The first (and dominant) term of the summation in (8) obtains an extremum at time $0.5\ln(2)\tau$. Until this time, a density disturbance will develop; afterward, the perturbation experiences a nearly exponential decay. Since velocities have not been considered in this example, the growth cycle must be entirely due to the diffusive mechanism.

4. Biconstituent diffusion combined with convection

A system describing dry (no condensation) convection results from combining the two-dimensional versions of (1)–(4) with the two-dimensional Boussinesq vorticity equation

$$\frac{\partial\eta}{\partial t}+\mathbf{v}\cdot\nabla\eta=\frac{g}{\bar{T}^*}\frac{\partial T^*}{\partial x}+K\nabla^2\eta, \tag{9}$$

where $\eta=\nabla^2\psi=(\partial w/\partial x)-(\partial u/\partial z)$ is the horizontal vorticity, g the acceleration of gravity, ψ the streamfunction, w the vertical component of velocity, u the horizontal component of velocity, and the overbar represents a horizontal average.

When the classical perturbation technique for linearization is applied to this system, the forcing function in the virtual potential temperature equation (4) is neglected, because it is the product of perturbations. Thus the biconstituent-diffusive effect is ignored.

In order to examine biconstituent diffusion the total nonlinear set of equations must be solved. A convenient non-dimensionalization is $\psi=K\hat{\psi}$, $t=(d^2/K)\hat{t}$, $\theta=\Theta\hat{\theta}$, $Q=\hat{Q}=1+0.608q$, $(x,z)=d(\hat{x},\hat{z})$ where d is a "characteristic" length of the system. The convective system equations become

$$\frac{\partial\theta}{\partial t}+J(\psi,\theta)=\nabla^2\theta, \tag{10}$$

$$\frac{\partial Q}{\partial t}+J(\psi,Q)=\nabla^2Q, \tag{11}$$

$$\frac{\partial}{\partial t}(\nabla^2\psi)+J(\psi,\nabla^2\psi)=\beta\frac{\partial T^*}{\partial x}+\nabla^2(\nabla^2\psi), \tag{12}$$

$$T^*=Q\theta, \tag{13}$$

where

$$\beta=\frac{gd^3}{K^2},$$

$$J(a,b)\equiv\frac{\partial a}{\partial x}\frac{\partial b}{\partial z}-\frac{\partial a}{\partial z}\frac{\partial b}{\partial x}.$$

(The carets have been dropped from the dimensionless variables.)

Eq. (12) states that the streamfunction developed by biconstituent diffusion is directly proportional to both the density perturbation developed in the system and to the third power of the system's characteristic length. Moreover, it is inversely proportional to the square of the eddy diffusivity. The problem is to solve the nonlinear set of equations, subject to reasonable boundary conditions. Because the set is not tractable by presently known analytical methods, it is necessary to resort to finite-difference methods. A diffusion-lagged leapfrog time difference is used. The Jacobians are approximated by the Arakawa (1966) method. Linear spatial derivatives are computed by a centered analog and a line over-relaxation method is used to obtain the streamfunction.

5. Integration over an infinite domain

For a first demonstration of the effects of biconstituent diffusion, conditions similar to those used in Section 3 are modeled. The domain of integration is made infinite by applying cyclic conditions to all boundaries. An initially uniform virtual potential temperature T^* is assumed. The initial potential temperature is a sinusoidal perturbation superimposed on a uniform value. The domain is in an initially quiescent state. In non-dimensional form, these initial conditions are

$$T^*|_{t=0}=1, \tag{14}$$

$$\theta|_{t=0}=\frac{A}{\Theta}+\frac{1}{\Theta}\cos(kx+mz), \tag{15}$$

$$\psi|_{t=0}=0. \tag{16}$$

The parameters k and m again are the thermal perturbation's horizontal and vertical wavenumbers. The characteristic length d is the perturbation's wavelength related to the wavenumbers through

$$d=2\pi(k^2+m^2)^{-\frac{1}{2}}. \tag{17}$$

Results of the integration can be interpreted by examining the temporal development of the streamfunction's maximum modulus ($\psi_m=|\psi|_{\max}\beta^{-1}$) along with the evolution of the virtual potential temperature perturbation ($\Delta T=T^*_{\max}-T^*_{\min}$). For a symmetric perturbation, mass flux is directly proportional to ψ_m. Buoyancy forces, which drive any developed circulation, are proportional to ΔT.

Values of the system parameters A and Θ were set at 298 K and 300 K respectively, which are characteristic of atmospheric values. Integrations were performed with the characteristic length d varying from 14.1 to 2000 m, and the eddy coefficient K ranging from 10 to 100 m^2 s^{-1}. Time histories of ψ_m and ΔT for eight combinations of d and K were virtually the same and are shown in Fig. 2. When A and Θ were varied over a 5 K range, the computed values of ψ_m and ΔT differed by less than 5% from those plotted. However, when the eddy coefficient was set to zero, both ψ_m and ΔT remained identically zero, showing that the development results entirely from diffusion effects and not to computational readjustment of the initial fields.

The temporal history of the density perturbation is in good agreement with the virtual potential temperature perturbation developed by the non-advective diffusion equations. In Section 3, it was shown that when only biconstituent diffusion acts, a perturbation will grow up to a dimensional time of $0.5\ln(2)[K(k^2+m^2)]^{-1}$ or a non-dimensional time of 0.00877, followed by a quasi-exponential decay. In the convective system, the maximum ΔT occurs at non-dimensional time 0.0087, after which an almost exponential decrease occurs.

The streamfield undergoes a similar development. As expected, its maximum lags behind that of the

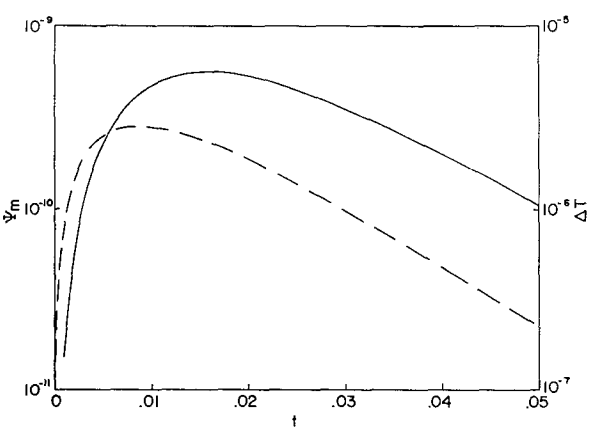

FIG. 2. Time variation of ψ_m (solid) and ΔT (dashed) for a cosine initial distribution.

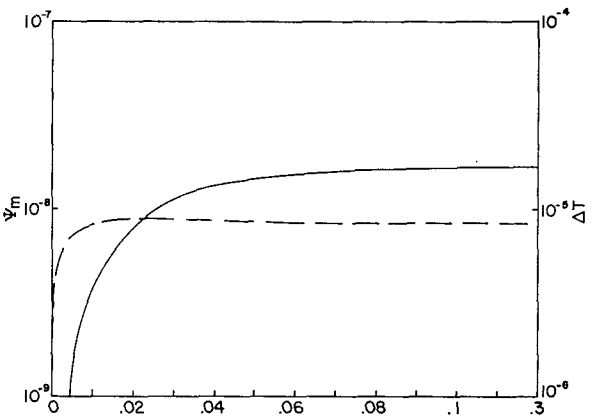

FIG. 3. Time variation of ψ_m (solid) and ΔT (dashed) for hyperbolic tangent initial distribution.

density perturbation and happens at a time of 0.0158. While the maximum virtual potential temperature anomaly is extremely small, the developed streamfield is surprisingly large. Vertical velocities rise to several centimeters per second at the time of maximum mass flux when reasonable values for d and K (2000 m and 10 m^2 s^{-1}, respectively) are chosen.

6. Sustained motions created by biconstituent diffusion

By limiting the domain of integration, through introduction of lateral boundaries, and by postulating more realistic initial distributions of heat and moisture, the diffusive mechanism induces much stronger, sustained motions. Consider two infinitely long impermeable vertical walls held at a constant potential temperature and mixing ratio. Between these boundaries the air is initially still with a uniform virtual potential temperature. It is composed of two isothermal masses of different potential temperature separated by a vertically-oriented transition zone. While the temperature and mixing ratio values are different along both walls, the density is horizontally uniform so that no "Margules" effect is present.

The initial distributions of the non-dimensional variables can be expressed as

$$T^*|_{t=0}=1, \tag{18}$$

$$\theta|_{t=0}=\frac{A}{\Theta}+\frac{P}{\Theta}\tanh\left[\frac{20}{d}\left(\frac{d}{2}-x\right)\right], \tag{19}$$

$$\psi|_{t=0}=0, \tag{20}$$

where d is the wall separation distance and P the potential temperature difference between the two isothermal regions. Vertical boundaries are treated as cyclic. A and Θ are again set to 298 K and 300 K, respectively. The half-amplitude P of the perturbation was set at 1 since any higher value would cause an un-

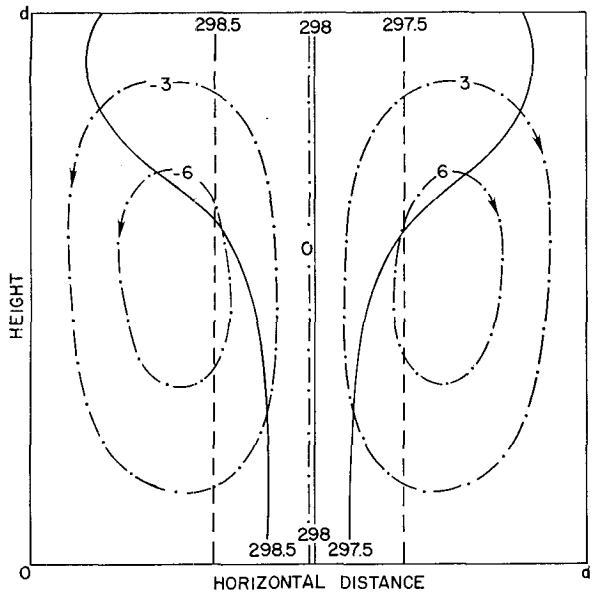

FIG. 4. Dimensional isentropes (K) for $d=2000$ m (solid), $d=20$ m (dashed), and the non-dimensional streamfield (dot-dashed) for a hyperbolic tangent distribution at $t=0.03$.

realistically large (>12 g kg^{-1}) mixing ratio difference across the domain.

Integrations were performed with d varying from 20 to 2000 m and K varying from 10 to 100 m^2 s^{-1}. As in the infinite domain case, the values of ψ_m and ΔT varied insignificantly with these changes. Fig. 3 is a graph of the temporal development of these parameters. Again with K set to zero, no development occurred.

The density anomaly again develops quite rapidly; by non-dimensional time 0.01 it is 93% of its maximum. However, in contrast to the totally cyclic example, the virtual potential temperature perturbation arrives at a quasi-steady state. This condition is possible because of the maintenance of the constant thermal and moisture conditions along the walls. To see this, consider the diffusion equations for moisture and heat in the non-advective limit. As time approaches infinity, both Q and Θ approach a steady state consisting of a linear distribution between the walls. However, the virtual potential temperature, which is the product of Q and Θ, approaches a quadratic form. Thus the density perturbation will not decay.

Similarly, the mass flux experiences a rapid increase. As time progress, the growth rate slackens but ψ_m continues to increase slowly in response to the nearly constant forcing of the density perturbation; ψ_m obtains values almost two orders of magnitude larger than its maximum in the totally cyclic case. Likewise, vertical velocities are much larger than previously. With d and K again fixed at 200 m and 10 m^2 s^{-1}, sustained vertical velocities of 40 cm s^{-1} are attained by non-dimensional time 0.12.

The streamlines from this integration are basically vertical (horizontal velocities are five orders of magnitude less than vertical ones). Since the initial potential temperature and mixing ratio fields only have a horizontal variation, the Jacobian terms are effectively eliminated from the diffusion equations (10) and (11). This makes the streamfunction directly proportional to the parameter β.

By now adding solid upper and lower surfaces which are insulated to both temperature and moisture, separated by the characteristic distance, closed circulations are induced within the interior of the domain (Fig. 4). This circulation causes an advective redistribution of the thermal and moisture fields. Since wind velocities are proportional to $(B/d)\psi$ [nondimensional], an increase of d by two orders of magnitude will increase the flow by four orders. The advective effect can be seen from Fig. 4 by comparing the dimensional potential temperature field produced with d set at 2000 m to that produced with a d of 20 m.

At time 0.03, the value of ψ_m has only changed by about 4% between the two experiments. With the large d, velocities are on the order of tens of centimeters per second; with the smaller d they are almost non-existent. Advective deformation of the insentrope field is very apparent. The isentropes bulge outward in the upper half of the domain and inward in the bottom half corresponding to the outflow and inflow from the updraft induced by the density perturbation.

7. Biconstituent diffusion near the dryline

An example of the biconstituent diffusive mechanism in the atmosphere is along the dryline. This synoptic feature is a very narrow, almost vertical zone across which a sharp horizontal moisture gradient occurs with no corresponding density gradient. The air exhibits a neutral stratification on the dry side, while an in-

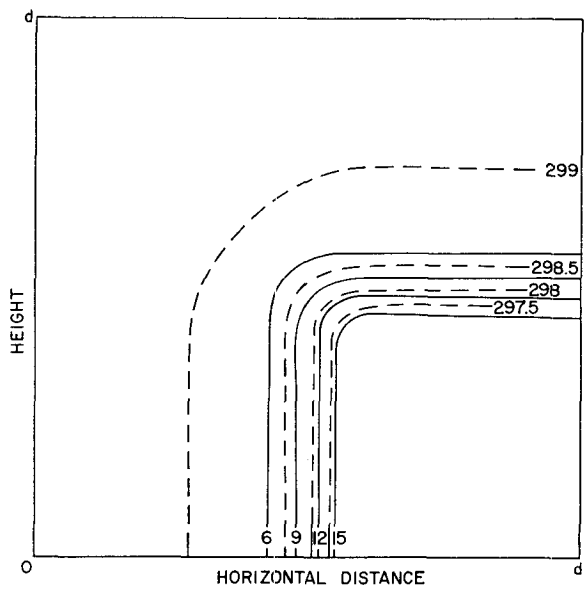

FIG. 6. Dimensional initial isentropes (K, solid) and isohumes (g kg^{-1} dashed), simulating a dryline.

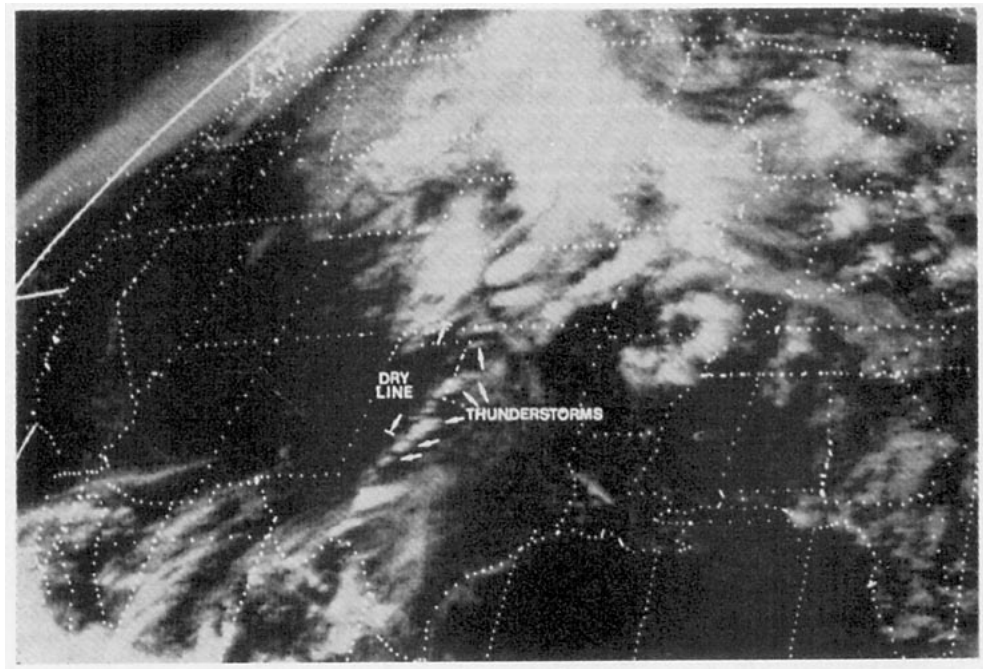

FIG. 5. Satellite photograph of a dryline in the eastern Texas Panhandle, at 2143 GMT 30 April 1972. Note the strong thunderstorms which have moved eastward off of the dryline, but the continued presence of the cumuliform cloud band along it.

version "caps" the moisture on the other side (Schaefer, 1974). Even though it is often not the zone of maximum surface convergence, the dryline serves as a focus for convective activity. A band of cumuliform clouds is often located over it. Some of these clouds can develop into quite strong thunderstorms that propagate eastward ahead of the dryline. Even after this occurs, clouds persist along the dryline (Fig. 5). This implies that the cloud line is a direct result of dryline presence and is not caused by quasi-random thermal convection.

To simulate the dryline phenomenon, the boundary conditions applicable to Eqs. (10)–(13) must be modified. Horizontal boundaries are assumed to be impermeable, insulating surfaces. Vertical boundaries are assumed reflective so that a solitary wave can be simulated in a finite domain. The initial distributions of the non-dimensional variables are expressed as

$$T^*|_{t=0}=1$$

$$\theta|_{t=0}=\frac{A}{\Theta}+\frac{1}{2\Theta}\left\{1+\tanh\left[\frac{20}{d}\left(x-\frac{d}{2}\right)\right]\right\}\times\left\{\tanh\left[\frac{20}{d}\left(z-\frac{d}{2}\right)\right]-1\right\},$$

$$\psi|_{t=0}=0,$$

where d is again the wall separation. With A and Θ set at 298 K and 300 K respectively, the dimensional initial distributions of potential temperature and mixing ratio are shown in Fig. 6.

When the equations are numerically integrated, rapid development of both a density perturbation and a closed circulation occurs (Fig. 7). ΔT again initially undergoes an explosive growth and then approaches a quasi-steady state, with ψ_m following with a slight lag. ψ_m values correspond to velocities of several tens of centimeters per second. The integration was stopped at non-dimensional time 0.03 to limit boundary contamination of the forecast fields. Without thermally fixed boundaries, the perturbation is free to move across the domain, and by this time was approaching the boundary.

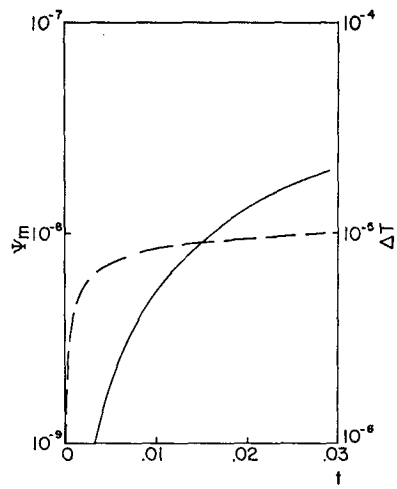

FIG. 7. Time variation of ψ_m (solid) and ΔT (dashed) for dryline simulation.

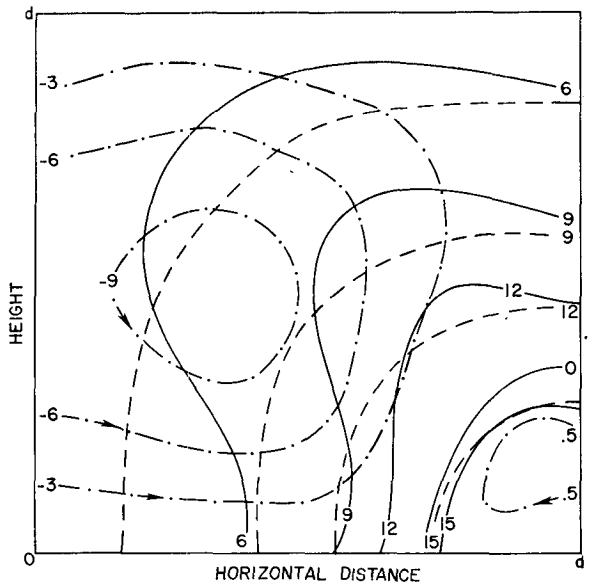

FIG. 8. Dimensional isohumes (g kg^{-1}) for $d=2000$ m (solid), $d=20$ m (dashed), and the non-dimensional streamfield (dot-dashed) in a dryline simulation at $t=0.02$.

The flow develops so that an updraft is centered over the dryline position (Fig. 8). With $d=200$ m, vertical velocities in this cell obtain magnitudes of several tens of centimeters per second. If precipitation physics (e.g., Soong and Ogura, 1973) were included, such a cell would produce convective clouds collocated with the dryline in a position corresponding to that observed in the atmosphere.

The rapid advective velocities produced by this cell are also quite important. In the absence of advection, the initial thermal and moisture gradients would be expected to diffuse and eventually spread across the entire domain. However, bioconstituent diffusion is quite significant, in that advection by the flow it induces helps to maintain the sharpness of the interface. [This finding agrees with recent speculations by Turner (1974) on possible atmospheric effects of double diffusion.] Fig. 8 also illustrates this effect. Isohumes at non-dimensional time 0.02 for integrations with $d=2000$ m and $d=20$ m are plotted. Also the non-dimensional streamfunction for the large d case is shown. At this instant, the maximum velocity for the large d case is 14 cm s^{-1} while it is 1.4×10^{-3} cm s^{-1} for the small β case. For the weak flow solution the moisture gradient has diffused considerably since the start of the integration. However, with the strong convective cell, the spreading has been considerably retarded. The diffusion-driven circulation enables the dryline to maintain itself. An induced convective circulation controlling the essential physics of a process is not unusual. "Spin-up" in a rotating fluid is similarly controlled by an induced secondary circulation (Greenspan, 1968).

Thus the process of biconstituent diffusion accounts not only for the dryline serving as a focus for convective development but can also account for the prolonged maintenance of the sharp dryline moisture gradient.

8. Concluding remarks

While this analysis of the biconstituent diffusion mechanism has been carried out under the extreme restrictions of eddy-coefficient theory and two-dimensionality, neither of these assumptions are necessary. They have only been made to simplify and clarify the complex nonlinear physical interactions. Any closure technique which allows eddy fluxes of heat and moisture to be independent of each other should yield similar results. Diffusion, which is generally considered dissipative, can actually rearrange constituents to transform potential energy into kinetic energy.

Acknowledgments. The author expresses his appreciation to his colleagues at NSSL, particularly Drs. R. Alberty, R. Davies-Jones and Mr. C. Doswell, who participated in discussions about the physics developed in this manuscript.

REFERENCES

Arakawa, A., 1966: Computational design for long-term numerical integration of the equations of fluid motions: Two-dimensional incompressible flow. Part I. *J. Comput. Phys.*, **1**, 119–143.

Baines, P. G., and A. E. Gill, 1969: On thermohaline convection with linear gradients. *J. Fluid Mech.*, **37**, 289–306.

Greenspan, H. P., 1968: *The Theory of Rotating Fluids.* Cambridge University Press, 327 pp.

Hill, G. E., 1974: Factors controlling the size and spacing of cumulus clouds as revealed by numerical experiments. *J. Atmos. Sci.*, **31**, 646–673.

Orville, H. D., and L. J. Sloan, 1970: A numerical simulation of the life history of a rainstorm. *J. Atmos. Sci.*, **27**, 1148–1159.

Purdom, J. F. W., 1971: Satellite imagery and severe weather warnings. *Preprints Seventh Conf. Severe Local Storms*, Kansas City, Mo., Amer. Meteor. Soc., 120–127.

Schaefer, J. T., 1973: The motion and morphology of the dryline. NOAA Tech. Memo. ERL NSSL-66, Norman, Okla., 81 pp.,

——, 1974: A simulative model of dryline motion. *J. Atmos. Sci.*, **31**, 456–964.

Schlichting, H., 1955: *Boundary Layer Theory*, 1st English edition, trans. by J. Kestin. McGraw-Hill, London, 535 pp.

Soong, S. and Y. Ogura, 1973: A comparison between axisymmetric and slabsymmetric cumulus cloud models. *J. Atmos. Sci.*, **30**, 897–893.

Turner, J. S., 1973: *Buoyancy Effects of Fluids.* Cambridge University Press, 367 pp.

——, 1974: Double-diffusive phenomena. *Annual Review of Fluid Mechanics*, Vol. 6, Palo Alto, Calif., Annual Reviews, Inc., 37–55.